Taxonomy of *Q*

Igor Morozov[1] and Amin Baharvand Ahmadi[1,2]

[1] University of Saskatchewan, Saskatoon, SK S7N 5E2, Canada

[2] Now at CGG, Calgary, AB Canada

ABSTRACT

The seismic quality factors (*Q*) used in many applications of exploration seismology are not automatically equivalent. We identify three groups of usage of the concept of a *Q*: 1) a measure of internal mechanical friction within rocks, as implied in petrophysical interpretations; 2) several types of apparent *Q* arising from attenuation measurements, and 3) axiomatic *Q* defined in the viscoelastic theory. These groups differ by their roles in the interpretation, sensitivity to model assumptions, frequency dependences, and particularly by the temporal and spatial resolution. Among all types of the *Q*, those which are most robust and useful for characterizing the material are also strongly limited in the resolution and accuracy. For example, White (1992) showed that to measure a *Q* of approximately 100 with modest accuracy of 30%, measurement time intervals of about 500 ms are required. Although several inversion techniques offer models of *Q* at much higher resolution, such detailed *Q* models are usually dominated by the effects of localized structures, such as 'colored' transmission across boundaries, reflectivity, or scattering. Such types of *Q* can be called 'structural', and they differ from the *Q*-factor of the medium. Detailed *Q* images are also sensitive to theoretical models such as background geometric spreading and assumptions about the frequency dependence of the *Q*. Direct association of such *Q*s with material properties may be inaccurate and unreliable. Measurement of geometric spreading and averaging of the 'structural *Q*' produce estimates of 'geometric' and scattering attenuation; however, these estimates are also strongly limited in accuracy and resolution. The viscoelastic *Q* (group 3 above) heavily relies on a specific mathematical model. Despite producing detailed images, the spatial resolution of viscoelastic *Q* is inherently limited by the nature of its relation to the frequency-dependent velocity. This resolution limit is difficult to assess quantitatively.

Taxonomy of Q

INTRODUCTION

Characterization of the ability of materials to absorb and dissipate seismic waves is important for petrophysical descriptions of reservoir rocks. Compared with seismic velocities and densities, absorption and scattering are often more sensitive to clay content, pore fluids, gas, or fracturing (e.g., Klimentos, 1995). Conventionally, energy dissipation properties are described by Q-factors attributed to the materials. However, despite their common name and intuitively expected similarity, the Q values encountered in different contexts are not automatically the same. In particular, we need to differentiate between three fundamentally different usages of the Q-factor: 1) the Q^{-1} as a measure of 'internal friction' implied in petrophysical interpretation, 2) many measured ('apparent') Qs arising from observations, and 3) the 'axiomatic', mathematical Q used in the viscoelastic theory and numerical modeling. A classification of these Q-factors can be constructed, based on the key properties of seismic attenuation (Figure 1).

In practical seismic data processing and inversion, the exact semantics of the Q is sometimes unimportant. The goal of attenuation modeling may be limited to correcting the data for its effects, and even a detailed Q model that is overparameterized, 'overfit' or not justified physically may work well by enhancing the data or aiding the interpretation. By contrast, when numerically modeling seismic wavefields, it is important to ensure that the algorithms adequately represent the physical mechanisms of wave attenuation. When a Q-type parameter represents the primary product of the analysis and is related to petrophysical properties, it is also important to ensure that it belongs to the 'internal friction' group in Figure 1.

The phenomenological aspect is critical for all three types of Q (Figure 1). The first of these types is the 'true', or 'material' Q, which represents the goal of attenuation analysis. In seismology and materials science, this Q is a property of the phenomenological 'imperfect modulus' (first column in Figure 1; Anderson and Archambeau 1964; Lakes, 2009), which is expected to comprise certain (petro)physical properties of the wave-propagating medium. These underlying properties may be broadly variable (for example, granularity, dislocations, fluid content, electrical, magnetic or thermal properties). The second, apparent Q (second column in Figure 1) is the common *tool* of attenuation analysis, empirical parameter reported from most observations. Apparent Qs may differ for different types of observations (for example, lab or field, refraction, reflection, or surface-wave), and their relation to the internal friction may be intricate and variable. The 'scattering Q' is an example of such a quantity that is particularly important in seismology and yet difficult to formalize and measure.

In contrast to the first two quality factors, the 'axiomatic' Q is attributed to the material mathematically, through the popular viscoelastic model (e.g., section 5.4 in Lakes, 2009). The purpose of this quantity is to represent the internal friction (material Q), but the approach consists in attributing phenomenological features, such as the relaxation times and strain-stress phase lags, to the viscoelastic moduli (Figure 1). As a mathematical model that is only an approximation for real internal friction, it occupies a separate place in our taxonomy (third

column in Figure 1). With models of the viscoelastic Q becoming progressively more detailed, their relation to the observations and physical properties of materials becomes intricate.

A classification of the concept of Q is a complex task because this concept represents a mixture of measurement techniques, empirical definitions, physical theories, mathematical transformations, simplifying assumptions, and analogies with mechanical and electrical resonators. In this paper, we discuss only several key aspects of this classification shown by ellipses in Figure 1. Our principal point is that the temporal and spatial resolution gives important important keys to such classification. By the nature of wave-attenuation phenomena and measurements, the kinds of Q useful for petrophysical correlations are *always averaged and statistical*, and therefore their accuracy and resolution in time and frequency are strongly limited (item 'c' in Figure 1). In a peculiar way, these restrictions apply even to the axiomatic, viscoelastic Q (item 'e'). White (1992) studied the statistical properties of spectral ratios and pointed out strong limitations on the Qs observed in common types of seismic measurements. The key lesson from White's paper was that in order to measure the values of $Q \approx 100$ with accuracy of about 30%, time intervals of at least ~500 ms need to be used for measuring the spectral ratios (White, 1992). However, many recent studies report Q images with much greater detail (for example, Frazer et al., 1997; chapters 11 and 12 in Wang, 2008; Blias, 2012; Suzuki and Matsushima, 2013). As some of these results appear to contradict White's (1992) statistical limits, an analysis of these contradictions seems appropriate. Fine-scale Q images are typically obtained at the cost of increased frequency dependence, sensitivity to mathematical assumptions, and even limited or difficult to assess physical meaning.

TAXONOMY OF Q

The apparent Q (second column in Figure 1) is the most important for the attenuation problem. This Q arises by considering a traveling wave whose spectral amplitude exponentially reduces with travel time, t, as (e.g., Aki and Richards, 2002):

$$A(f,t) = A_0(f,t)\exp\left(-\pi f \int_0^t dt'/Q\right), \tag{1}$$

where $A_0(f,t)$ is the signal spectrum including all geometric-spreading, source, and receiver effects. Note that under the term 'geometric spreading', we understand all propagation effects *in the absence of attenuation*, and not merely the ray-theoretical limit. Furthermore, the term 'attenuation' is understood as all physical mechanisms causing wave amplitude reduction within the material, in contrast to wavefront spreading for an idealized, 'geometrical' wave modeled by $A_0(f,t)$. The path attenuation factor $t^* \equiv \int_0^t (dt'/Q)$ in the exponent of expression 1 is often used in body-wave analysis (Der and Lees, 1985). The justification for the existence of t^* or Q as attenuation properties is based on common observations that the negative exponent in the amplitude-decay expression 1 increases with f and accumulates with t.

In relation 1, the notions of Q and t^* are relative and vary with the detail of the background model $A_0(f,t)$ (item 'a' in Figure 1; Morozov, 2010a, hereafter M10a and similarly other papers by Morozov). For example, with typical simple models for geometric spreading, the

exponential factor in equation 1 approximates the effects of additional curvatures of the wavefronts and wavelet dispersion associated with scattering on small heterogeneities (M10a, M11). Although these effects can always be included in a more detailed background model $A_0(f,t)$, they are variable spatially and can rarely be modeled with accuracy (of about Q^{-1}) required for attenuation measurements. Also, the notion of a waveform traveling along a certain "ray path" in relation 1 becomes invalid for multiple scattering and dispersive wavelets. Hence, the uncertainty and variability of the geometric spreading is contained in Q and t^*, and it needs to be measured as discussed below.

Because there is no attenuation at zero propagation time, the limit $A(f,0) \equiv A_0(f,0)$ in relation 1 is always correct. Nevertheless, the low-frequency limit $A(0,t) \equiv A_0(0,t)$ that is also implied by this relation is not guaranteed. For example, for scattering or small deviation of the geometric spreading from the background model, there exists a frequency-independent deviation of *A* from A_0 increasing with travel time (M11). To allow $A(0,t) \neq A_0(0,t)$ without a singularity in $Q(f)$ at low frequencies, we extended the model 1 by adding a frequency-independent attenuation coefficient γ (M08):

$$A(f,t) = A_0(f,t)\exp\left[-\int_0^t (\gamma + \kappa f) dt' \right]. \tag{2}$$

Here, κ measures the frequency-dependent part of attenuation that can be transformed into the 'effective' *Q*-factor: $Q_e \equiv \pi/\kappa$ (M08, M10a). In the following, we will not differentiate between the Q_e and *Q*. Parameter γ can be interpreted as 'geometric' attenuation including small wavefront distortions (focusing for $\gamma < 0$ or defocusing for $\gamma > 0$) and/or random scattering (for which $\gamma = g_0 V/2$, where g_0 is the turbidity (measure of random heterogeneity of the medium, and *V* is the wave velocity; Dainty, 1981; M08). Parameter κ is phenomenological and can generally be frequency-dependent. However, in practice, a constant κ typically appears sufficient (M08, M10a, M10b; Baharvand Ahmadi and Morozov, 2013, hereafter BAM13). Thus, instead of the (generally) frequency-dependent *Q* in relation 1, we have a two-parameter model 2.

In the following section, we focus on several aspects of this classifications indicated by the ellipses in Figure 1 and make four general observations about the different types of *Q*. First, the apparent attenuation (κ and γ combined) is always an averaged, statistical effect accumulated over time (exponent in equation 2; item 'c' in Figure 1). Because of such averaged character, measurements of attenuation always require a sufficient volume of time-spectral data, which restricts the temporal resolution of attenuation properties. Phenomenological parameters such as γ, κ, and *Q* are statistical attributes which simply do not exist on short temporal and spatial scales. Following White (1992), we show that there exists a significant trade-off between the accuracy of the measured values of γ and κ (aka *Q*) and their temporal resolution. White's (1992) and our estimates of the attainable resolution (further in this paper) are summarized in Table 1.

Second, we note that whenever the parameterization of models 1 or 2 is insufficient for matching the real amplitude decay $A(f,t)$, a 'frequency dependence of *Q*' appears (item 'a' in

Figure 1). A frequency-dependent Q may thus be often caused by an inadequacy of the parameterization and not by a physical reality. The frequency dependences of Q measured in an experiment depend on whether the models 1 or 2 are used (M10a). In many studies, it is customary to *assume* that $\gamma = 0$ and consequently use equation 1. This assumption is usually offered as a simplification and implies that the geometric spreading in $A_0(f,t)$ is accurate enough to allow the measurement of κ. However, examples from many seismic datasets (M08, M10a, M10b; BAM13) and numerical modeling (Morozov et al., 2008) show that this assumption is often inaccurate or impractical. Once invoked, this assumption can cause spurious frequency dependences in $Q(f)$ (M08, M10a). Therefore, for practical measurements of seismic Q, it is important to see that the assumption of $Q(f) = $ const *is inconsistent* with also assuming $\gamma \equiv 0$.

Our third observation relates to the character of detailed Q models that appear to sometimes overcome the statistical limitations (for example, wavelet-based Q models in chapter 11 by Wang, 2008; interval Q model in Blias, 2012; sonic-log Q in Suzuki and Matshushima, 2013). These models also relate to special kinds of the apparent Q (item 'b' in Figure 1). We argue that physically, such models represent short-scale variations not of a quality factor but of 'colored' transmitted and/or reflected seismic amplitudes. This apparent Q can therefore be called 'structural Q' (Figure 1). To associate this Q with a robust property of the material, we again need to perform averaging and accumulate sufficient statistics. This averaging produces the well-known 'scattering Q' (Dainty, 1981), which also exhibits resolution/accuracy limitations similar to those from spectral-ratio measurements (Table 1). In addition, both the structural Q and scattering Q may be frequency dependent if the assumption $\gamma = 0$ is made.

Fourth, very detailed Q models arise from full waveform inversion (Virieux and Operto, 2009). This type of Q is the 'axiomatic' Q inferred from the viscoelastic model of attenuation (item 'e' in Figure 1). However, the viscoelastic Q is not the only, and arguably not the most rigorous and accurate model of internal mechanical friction within solids (Landau and Lifshitz, 1986). Although reproducing the general effect of attenuation (relations 1 and 2), such Q may be difficult to interpret (petro)physically. Despite the detailed spatial sampling of this Q, we show that a peculiar 'averaging' is also implied in its definition (item 'd' in Figure 1). In addition, waveform Q tomography also often uses the assumptions of $\gamma = 0$ and $Q = $ const simultaneously. Similarly to the above, such combined assumptions may bias the resulting Q values.

With regard to the Q as a true material property, its universal existence for rocks and frequency dependence are open to debate and not discussed here (symbols '?' in Figure 1). Rigorous models of internal friction in materials, such as poroelasticity, thermoelasticity, or viscosity, contain no material Q but explain the wave attenuation directly (Landau and Lifshitz, 1986). Theoretical models of laboratory measurements of seismic attenuation (Coulman et al., 2013) also show that the apparent Q is not always a true property of the material and may depend, for example, on the shapes and dimensions of the specimens.

Finally, no classification of Q is complete without considering the intrinsic and scattering Qs. These quantities are defined by partitioning the observed (apparent) Q (e.g., Wu, 1985):

$$Q^{-1}_{observed} = Q^{-1}_{intrinsic} + Q^{-1}_{scattering}. \tag{3}$$

The intrinsic-energy dissipation rate $Q^{-1}_{intrinsic}$ describes the dissipation of the elastic-wave energy into heat, whereas the elastic dissipation rate $Q^{-1}_{scattering}$ corresponds to the fraction of energy remaining in the total field but diverted from the recorded wavelet by scattering. By an analogy with optics, quantity $Q^{-1}_{scattering}$ is sometimes called "extrinsic attenuation" (e.g., Virieux and Operto, 2009). A similar additive rule for Q^{-1} was used for combining the effects of an anelastic dry rock matrix and mesoscopic fluid flow in a fluid-saturated rock (Tisato et al., 2014). Many methods were developed to separate the two terms in equation 3 (e.g., Aki, 1969; Wu, 1985).

In our taxonomy, both $Q^{-1}_{intrinsic}$ and $Q^{-1}_{scattering}$ are placed under the apparent-Q category, similarly to $Q^{-1}_{observed}$ (ellipse 'b' in Figure 1). This may appear surprising, as the intuitive meaning of $Q^{-1}_{intrinsic}$ is that of an intrinsic energy loss, i.e. internal friction. However, the separation of these two quantities uses no specific physical model for $Q^{-1}_{intrinsic}$ which could indeed relate this quantity to the generation of heat. The separation of these Qs is entirely based on the model for scattering, which depends the assumed single or multiple scattering, geometric spreading, and distribution of scatterers (Wu, 1985; M11). The values of $Q^{-1}_{scattering}$ can therefore be treated as apparent. Neither $Q^{-1}_{intrinsic}$ nor $Q^{-1}_{scattering}$ exist at the microscopic scale, which also suggests that they are not 100% material properties. Thus, the quantitative definition and separation of these quantities represents a complicated problem, and it is not considered further in this paper. This problem does not affect the discussion of the resolution and accuracy of Q in this paper.

PROPERTIES AND TYPES OF Q

Accuracy and temporal resolution

In this section, we consider the characteristic temporal resolution common to most types of the apparent attenuation (item 'c' in Figure 1). Consider the task of estimating γ and κ in process 2 from discrete seismic-amplitude data samples. For a specific case, consider a borehole measurement, such as seismic VSP or acoustic well log recorded with a constant source spectrum $A_0(f)$. This type of measurement provides the highest statistical accuracy (White, 1992). To assess parameters γ and κ in equation 2, we need to measure the amplitude spectra within two time windows of length T and separated by time t. Let us sample the spectra at N equidistant frequencies f_i taken within a frequency band of width B. The estimates for γ and κ, denoted $\hat{\gamma}$ and $\hat{\kappa}$, can be obtained by fitting a linear regression to the logarithms of the amplitude spectral ratio for the two time windows, $A_2(f)/A_1(f)$:

$$\frac{1}{t}\ln\left(\frac{\hat{A}_{2i}}{\hat{A}_{1i}}\right) = -\left(\hat{\gamma} + \hat{\kappa}f_i\right), \tag{4}$$

The estimates $\hat{\gamma}$ and $\hat{\kappa}$ derived from this regression are random quantities dependent on the sampling of the spectra and possess statistical errors. Considering high-quality records with signal to noise ratio much higher than one and measurements within independent time windows, the relative variance of the spectral ratio equals (White, 1992):

$$\frac{\text{var}\left\{\left|\hat{A}_2(f)/\hat{A}_1(f)\right|\right\}}{\left|\hat{A}_2(f)/\hat{A}_1(f)\right|^2} = \text{var}\left\{\ln\left|\hat{A}_2(f)/\hat{A}_1(f)\right|\right\} = \frac{1}{2bT}, \tag{5}$$

where b is the bandwidth of each frequency reading. Approximating this variance as constant within the measurement bandwidth and assuming that the full frequency band is utilized ($B = Nb$), the variances of the estimates $\hat{\gamma}$ and $\hat{\kappa}$ determined from regression 4 equal:

$$\frac{\text{var}\{\hat{\gamma}\}}{\gamma^2} \approx \frac{1}{\gamma^2 t^2 2BT}, \text{ and } \frac{\text{var}\{\hat{\kappa}\}}{\kappa^2} \approx \frac{6\left(1-\Gamma^2\right)}{\kappa^2 t^2 B^3 T}, \tag{6}$$

where Γ^2 is the spectral coherence of the records. The second of these expressions is equation 22 in White (1992).

The relative standard error of $\hat{\gamma}$ and $\hat{\kappa}$ (here denoted e_γ and e_κ respectively) equal square roots of the ratios 6. These relations show that e_γ and e_κ trade off with t. If we wish to achieve certain levels of these errors, then the spectral measurement windows should be separated by at least the time interval

$$t \geq \frac{1}{\sqrt{BT}} \max\left\{\frac{1}{|\gamma|e_\gamma\sqrt{2}}, \frac{\sqrt{6\left(1-\Gamma^2\right)}}{\kappa e_\kappa B}\right\}. \tag{7}$$

This constraint restricts the time resolution attainable in attenuation measurements and shows that it inversely correlates with $|\gamma|$, κ, e_γ and e_κ.

For a representative example, consider a 3-C VSP in the area of Weyburn reservoir in Saskatchewan, Canada (BAM13). This study resulted in high-quality first arrivals (Figure 2), from which a six-layer, anisotropic model was derived for γ and κ (BAM13). The first-arrival measurement intervals were $T = 60$ ms (Figure 2a). Let us take the bandwidth of the data as ranging from 10 to 90 Hz, and therefore $B = 80$ Hz. The spectral coherence of the first arrivals within this frequency band exceeds 99% and generally decreases with time separation between the first-arrival VSP waveforms, which is shown by the increasing 'incoherence' factor $\sqrt{1-\Gamma^2}$ in Figure 3. Note that this quantity increases near the bottom of the borehole, where the reflectivity is much stronger (increased velocity and density variation within layer 6 in Figure 2b and c and gray dots in Figure 3). For a simple estimate, let us approximate as $\sqrt{1-\Gamma^2} \approx a + bt$

(dashed line in Figure 3) and denote $c \equiv \sqrt{6}/\left(\kappa e_\kappa B\sqrt{BT}\right)$. The second constraint 7 then becomes:

$$t \geq ca/(1-cb). \qquad (8)$$

For near-vertical wave propagation, the levels of $|\gamma|$ in BAM13 ranged from ~0.3 s^{-1} to ~3 s^{-1}, and κ ranged from 0.02 (corresponding to $Q_e \approx 160$) to 0.13 ($Q_e \approx 24$). Taking conservative target errors of $e_\gamma = e_\kappa = 0.3$, the shortest intervals t required for measuring the above two levels of γ equal 3.6 s and 360 ms, respectively (Table 1). For the two levels of κ above, relations 8 give $t \geq 170$ ms and $t \geq 12$ ms, respectively. For $Q = 50$ ($\kappa \approx 0.063$), this limit would be $t \geq 27$ ms (Table 1).

Thus, measurements of attenuation (γ, κ, and accordingly Q) cannot be both very detailed and accurate even with high-quality first-arrival VSP records. Measuring γ appears to be practical only with little spatial detail and statistical accuracy. This is probably why this quantity is rarely measured. In BAM13, the relative errors in γ were close to or exceeded one, and its determination suffered from strong tradeoffs with errors in κ. Note that by using a broader bandwidth and higher coherence, the above estimates are significantly more 'optimistic' than White's (1992), but they are still quite restrictive (Table 1). The relative errors in γ, κ and Q decrease with time intervals as $1/t$ and $1/\sqrt{T}$ and with the frequency bandwidth as $B^{-1/2}$ for γ and $B^{-3/2}$ for κ.

Interval and structural Q

Many measurement methods are technically capable of producing estimates of Q^{-1} that are much more detailed than the statistical limits in Table 1. For example, Q modeling and compensation based on wavelet transforms can produce detailed layering of Q (e.g., chapter 11 in Wang, 2008). The common-spectrum method (Halderman and Davis, 1991), rise-time and instantaneous-frequency methods (Matheney and Nowack, 1995) can in principle yield trace-by-trace Q estimates. The mean-median procedure (Frazer et al., 1997; Sun and Frazer, 2000; Suzuki and Matsushima, 2013) also derives very detailed layering of Q^{-1} from sonic waveform logs. Optimization approaches using relations 1 or 2 also produce interval-Q models (e.g., Blias, 2012) that may be much more detailed than allowed by the statistical limits (Table 1). However, such detailed Qs are somewhat *different* phenomenological measures of wave attenuation that need to be understood carefully. These Qs represent examples of model-dependent apparent attenuation indicated in the ellipse 'b' in Figure 1.

In the preceding section, we only discussed the limits imposed on the accuracy of attenuation measurements by fluctuations in spectral sampling. However, there also exist fluctuations due to limited spatial sampling of the target zone. For interval Q measurements such as VSP and sonic logging, these fluctuations affect the attenuation-free amplitude $A_0(f,t)$ in equation 1. This $A_0(f,t)$ becomes complex, 'colored' (frequency-dependent), and variable when selecting different depth intervals or spatial areas for the measurements. The $A_0(f,t)$ is mostly

caused by reflectors and velocity variations within and near the measurement range. In sonic-log measurements, the receivers may also be close to the near-field zone, in which the amplitude spreading changes from $1/r^2$ to $1/r$ and is frequency-dependent. With the conventional $1/t$, $1/V^2t$, $t^{-\alpha}$, or in fact any other modelled corrections for the geometric spreading, the residual 'colored' response in $A_0(f)$ contributes to the κ (i.e., Q) results (M10a). Suzuki and Matsushima (2013) note that Q^{-1} measured in these cases mostly represents the scattering on the layered structure of the reservoir. However, for each position of the sonic tool, this structure is unique and typically dominated by 1–2 strong reflectors. Such situations can be described as fluctuations of scattering and the resulting Q-factor called the 'structural Q'. However, the use of the Q-factor for characterizing the structure is still hardly appropriate and can be tricky. It is very difficult to pinpoint a combination of physical properties (especially *material* properties) that may be related to this Q.

Frequency dependence of Q

Figure 5b illustrates the dependence of the apparent Q on the assumed background model in our VSP example (observation 'a' in Figure 1). If scattering Q_s is defined without a γ, by assuming $A \propto \exp\left(-\pi ft/Q_s\right)$ in the empirical law 1 (Aki, 1969), then it quickly increases with frequency. In our example, Q_s increases from ~850 at 10 Hz to ~1700 at 100 Hz (dotted lines in Figure 5a). If using the model 2, then the scattering Q would be approximately $Q_s = \pi/\kappa_s \approx 2400$. Thus, for methods relying on explicit corrections for theoretical models of the attenuation-free response $A_0(f,t)$ in expression 1, *we should always expect* the resulting $\hat{\kappa}$ and Q to be frequency-dependent (M08). Unfortunately, this frequency dependence is often attributed to the 'material Q' (symbols '?' in Figure 5b), but in fact it may be caused by the selected parameterization 1 and inaccurate models for geometric spreading.

The frequency dependence for the phenomenological Q produced by an error in γ can be obtained from expression 2:

$$Q^{-1}(f)=\left(1+\frac{f_c}{f}\right)Q_\infty^{-1},\tag{9}$$

where the ray-theoretical limit (at $f \to \infty$) is denoted $Q_\infty^{-1} \equiv \kappa/\pi$, and $f_c \equiv \gamma/\kappa$ is the 'crossover frequency' (M08). This expression shows that weak frequency-independent scattering or wavefront defocusing ($\gamma > 0$) cause a Q nearly proportional to f when measured at frequencies $f \gg f_c$. Such strong positive $Q(f)$ dependences are often reported in earthquake studies (e.g., Aki, 1969). Nevertheless, such frequency dependences only apply to the apparent Q (Figure 1) and arise when the restrictive assumption $\gamma = 0$ is made. When this assumption is relaxed, the $Q(f)$ often becomes near-constant, and its values at $f = 1$ Hz increase 20–30 times (M08, M10a).

Scattering *Q*

'Scattering *Q*' is another kind of apparent *Q* measured in random wavefields, such as the seismic coda (item 'b' in Figure 1; Aki, 1969). In this section, we try estimating the time intervals needed for measuring this *Q* in exploration-type data. The scattering *Q* can be viewed as averaging of the 'structural *Q*'. To illustrate this averaging on the above VSP example, we modeled harmonic P-wave responses in a layered structure simulated by using the complete well logs recorded in the same area (Figure 2; BAM13). The downgoing wave was normalized to a flat spectrum at depth 431 m, and its attenuation to the level of 690 m was measured (Figure 4). Note that this model is purely elastic, and therefore the results relate to the pure 'structural *Q*'. In relation to the statistical discussion in the preceding section, note the significant thickness of the depth interval (259 m, corresponding to about 118 ms of one-way travel time).

From a single observation (the only one we ever have with real data!), the near-linear spectral slope is apparent, but significant fluctuations are present in it as well (thick black line in Figure 4a). The transmitted response and attenuation parameters change when the layers are randomly permuted within this depth interval (gray lines in Figure 4a). Thus, the layering causes significant fluctuations with respect to random sampling of the same (even elastic) strata. By using a representative set of permutations, the fluctuations are averaged out, and the 'scattering *Q*' and the covariance of $\hat{\gamma}$ and $\hat{\kappa}$ values can be measured (large dot in Figure 4b). If desired, the pair of parameters γ_s and κ_s can be replaced with a 'frequency-dependent scattering *Q*' as $Q(f) = \pi f / (\gamma_s + \kappa_s f) \approx Q_0 f^{\eta}$, with another pair of parameters Q_0 and η (M08). The errors of the scattering parameters are correlated and equal approximately ± 0.04 s^{-1} (for γ_s) and $\pm 10^{-3}$ (for κ_s) (ellipse in Figure 4b). For simplicity, the uncertainty is estimated here by 'eyeballing' the distribution of (γ, κ) points, so that the error ellipse contains approximately 80% of this distribution.

The 'scattering *Q*' (the large dot in Figure 4b) only becomes available after about 5–10 randomizations of the layer. This suggests that in a real dataset, a 600–1200-ms one-way time interval would be needed for assessing these values (Table 1). For comparison, in earthquake seismology, the scattering *Q* is commonly derived by using coda lengths of twice the total direct S-wave travel times, which amounts in 30–60 wavelengths (Aki, 1969; Dainty, 1981). At exploration frequencies (~40 Hz), such averaging would correspond to 700–1400-ms time intervals, similar to the preceding estimates for κ and γ (Table 1). Unfortunately, such thicknesses appear hardly practical in most cases.

Note that the spectral slope measured before layer permutations ($\kappa_{\text{raw}} \approx 6 \cdot 10^{-3}$; Figure 4a) is much greater than that in randomized logs ($\kappa_s \approx 1.3 \cdot 10^{-3}$) and lies outside of the 80% confidence ellipse (Figure 4b). This difference occurs because the original layering is non-random, as also indicated by the spectral density of reflectivity increasing with frequency (Figure 5a). The difference between κ_{raw} and κ_s corresponds to the difference between the 'structural' and scattering *Q*-factors. Also note that in principle, Q_s can be redefined to incorporate the finite correlation lengths and other spectral properties of the logs.

The random permutations also reveal another observation showing that scattering may not fit into any simple Q-type models. The frequency dependence of the averaged energy flux suggests a quadratic dependence of the amplitude on the frequency as $A \propto \exp\left[-\left(\gamma + \kappa f + \vartheta f^2\right)t\right]$ rather than linear $A \propto \exp\left[-\left(\gamma + \kappa f\right)t\right]$ in relations 1 and 2 (Figure 5b). This trend correlates with the near-quadratic spectral power of reflectivity (Figure 5a; O'Doherty and Anstey, 1971). Thus, linear Q models of types 1 and 2 may be insufficient for scattering in finely layered sedimentary sequences.

Viscoelastic ('axiomatic') Q

In this section, we discuss the 'axiomatic' Q (items 'd' and 'e' in Figure 1). Several theoretical models explain dissipation of elastic waves in solids, such as poroelasticity (Biot, 1956), squirt pore-fluid flows, thermoelasticity, and solid viscosity (Landau and Lifshitz, 1986). These physics-based models belong to the 'internal friction' category in Figure 1. Another theoretical approach to anelastic attenuation is represented by the viscoelasticity (Aki and Richards, 2002; Lakes, 2009). Because of its simplicity and generality, this model is broadly used in exploration and observational seismology and lab studies.

In the viscoelastic model, the observations of internal friction are explained by a specialized parameter (viscoelastic Q) associated with the elastic modulus. This parameter combines the properties of the apparent Q with the localization and 'reality' of the physical internal friction (first two columns in Figure 1). Similarly to the modulus, the viscoelastic Q is free from the statistical constraints discussed above, and its images can be arbitrarily detailed. For example, to explain wave attenuation in porous rock containing heavy oil or melts, viscoelastic moduli and Qs are attributed to pore fluids or solids, i.e. to the microscopic level (Mavko, 2013). Nevertheless, the viscoelastic model still does not automatically correspond to reality (see below), and its Q should be differentiated from the internal friction and the various apparent Qs (Figure 1).

In the attenuation waveform tomography, the viscoelastic Q is derived from the complex-valued wave velocity, c^* (Aki and Richards, 2002):

$$Q^{-1} = -\frac{2\,\mathrm{Im}\,c^*}{\mathrm{Re}\,c^*}. \tag{10}$$

Because typically $Q^{-1} \ll 1$, the inversion for Q^{-1} is an ill-posed problem and needs to follow careful strategies, such as first solving for $\mathrm{Re}c^*$ and then fitting the data residual by adjusting only $\mathrm{Im}c^*$ (Virieux and Operto, 2009, and references therein). Because the resulting Q^{-1} represents a transformation of complex-valued velocities, it has the resolution of a velocity image.

Nevertheless, even though computed at every model point, the viscoelastic Q^{-1} in equation 10 is still inherently 'averaged' in a peculiar sense that is rather difficult to understand physically. To recognize this averaging, note that relation 10 implies the Kolsky-Futterman model for the frequency dependence of c^* (Virieux and Operto, 2009):

$$c^*(\omega) = \frac{c}{\left(1 + \dfrac{1}{\pi Q}\left|\ln\dfrac{\omega}{\omega_r}\right|\right) + i\dfrac{\mathrm{sgn}\,\omega}{2Q}} \, , \tag{11}$$

where ω_r is some reference frequency, and ω is the observation frequency. In this model, the velocity c is the *phase velocity* of a harmonic wave *in a uniform medium*, and the Q^{-1} is the *apparent attenuation factor* for this wave (Aki and Richards, 2002). Extrapolating this expression to a local wave speed and local internal friction within a heterogeneous body is an extremely far-reaching mathematical postulate known as the correspondence principle (Lakes, 2009). Without discussing the relation of this principle to physics, we only note that the Q^{-1} in equation 10 actually refers to plane waves in some 'equivalent', infinite and uniform medium whose parameters equal those at a single point selected in the model (Figure 6). This means that equation 10 is only guaranteed and accurate for an unbounded uniform medium. However, the Q^{-1} of a wave in this medium is not automatically the same as the path-average Q^{-1} in the real world or in the ray-based equation 1.

In addition, as in the preceding sections, when using the usual imaging condition $Q^{-1} = const$ (Wang, 2008), we should not assume $\gamma = 0$. When taking $\gamma = 0$ (as commonly done), the right-hand side of expression 10 should become frequency-dependent, which should bias the resulting values of Q^{-1}. An apparently better alternative to expression 10 for waveform attenuation tomography could be:

$$\frac{2\gamma}{\omega} + \kappa = -\frac{2\,\mathrm{Im}\,c^*(\omega)}{\mathrm{Re}\,c^*(\omega)} \, , \tag{12}$$

which would be consistent with equation 2. An inversion for both γ and κ would produce an interesting pair of attributes of the phase-shifted complex velocity field which could potentially be of some petrophysical value. However, it still remains to be studied whether and how these attributes are related to the phenomenological attenuation properties γ and κ (and Q) in Figure 1. In any case, quantities γ and κ (Q) in equations 12 and 2 should not be automatically equated, despite the similarity of notation and equations.

DISCUSSION AND CONCLUSIONS

The measures of seismic attenuation used in different models and obtained from different measurements and inversion approaches are not automatically equivalent. We identify three groups of such measures differing by physical meanings, underlying theories, methods of measurement, attainable resolution and accuracy, and most importantly, by their roles in data analysis and interpretation (Figure 1) .

From the above descriptions of the different aspects of the Q, it follows that most of the existing estimates of Q belong to the 'apparent' Q category and not to the internal friction (i.e. representing a material property) as it may be implied (Figure 1). Moreover, these values are only robust (as 'interval' or 'scattering' Q in contrast to the 'structural Q') when averaged over

substantial time and/or spatial intervals. We suggest that such statistical, averaged character is an important characteristic of any self-consistent type of a Q.

Because of its averaged character, the resolution and accuracy of the phenomenological Q is limited. We confirm and reiterate the conclusion by White (1992) that to measure a $Q \approx 100$ in VSP first arrivals with reasonable accuracy, we need to use time intervals of about 500 ms (Table 1). In addition, the measured Q values may be non-unique and depend on the adopted geometric-spreading and/or frequency-dependence models. In particular, errors in geometric spreading cause Q values to quickly decrease at low frequencies. This model dependence can be relieved by measuring the geometric spreading and scattering; however, such measurements are even more challenging, with likely uncertainties reaching 100%.

Many fine-scale Q models exceed the above statistical resolution limits, which suggests that these Qs are likely influenced by deterministic local structures. An example of such a 'structural' Q from borehole log studies suggests that such phenomena should better not be treated as a Q. The apparent structural Q contains effects of 'colored' transmission and reflections on layered structures, as well of the underlying theoretical models. Detailed models should always be based on first-principle analysis and utilize specific, spatially localized and unambiguous physical properties rather than a Q.

The traditional viscoelastic Q occupies a separate category in our taxonomy (Figure 1). By construction, this Q combines the time- and frequency-dependence properties of the apparent Q with the constitutive character of an 'internal-friction' model. We point out that although this model is convenient mathematically, broadly used and seems intuitively appealing, its rigorous meaning and relation to petrophysical properties is poorly understood. The viscoelastic model also contains a specific, inherent spatial averaging that is difficult to assess in Q images.

Finally, the true internal-friction mechanisms (first column in Figure 1) are usually explained by first-principle physics and generally do not require the notion of a Q. Their relations to Q models can be complicated and require further studies.

ACKNOWLEDGMENTS

REFERENCES

Aki, K., 1969, Analysis of the seismic coda of local earthquakes as scattered waves: Journal of Geophysical Research, **74**, 615–631.

Aki, K., and P. G. Richards, 2002, Quantitative Seismology: Second Edition: University Science Books.

Anderson, D. L., and C. B. Archambeau, 1964, The anelasticity of the Earth, Journal of Geophysical Research, **69**, 2071–2084.

Baharvand Ahmadi, A., and I. Morozov, 2013, Anisotropic frequency-dependent spreading of seismic waves from first-arrival vertical seismic profile data analysis: Geophysics, **78**, C41–C52. doi: 10.1190/geo2012-0401.1

Biot, M. A., 1956, Theory of propagation of elastic waves in a fluid-saturated porous solid, II. Higher-frequency range: Journal of Acoustical Society of America, **28**, 168–178.

Blias, E., 2012, Accurate interval Q-factor estimation from VSP data: Geophysics, **77**, WA149-WA156.

Carcione, J. M., 1992, Anisotropic Q and velocity dispersion of finely layered media: Geophysical Prospecting, **40**, 761-783.

Coulman, T., W. Deng, and I. Morozov, 2013, Models of seismic attenuation measurements in the laboratory: Canadian Journal of Exploration Geophysics, **38**, 51-67.

Dainty, A. M., 1981, A scattering model to explain seismic Q observations in the lithosphere between 1 and 30 Hz: Geophysical Research Letters, 8, 1126-1128.

Der, Z. A., and A. C. Lees, 1985, Methodologies for estimating $t^*(f)$ from short-period body waves and regional variations of $t^*(f)$ in the United States: Geophysical Journal Royal of Astronomical Society, **82**, 125–140.

Frazer, L. N., X. H. Sun, and R. H. Wilkens, 1997, Changes in attenuation with depth in an ocean carbonate section: Ocean Drilling Program sites 806 and 807, Ontong Java Plateau: Journal of Geophysical Research, **102**, 2983–2997, doi: 10.1029/96JB03189.

Halderman, T. P., and Davis, P. M., 1991, Q_p beneath the Rio Grande and East African Rift zones: Journal of Geophysical Research, **96**, 10113-10128.

Klimentos, T., 1995, Attenuation of P- and S-waves as a method of distinguishing gas and condensate from oil and water: Geophysics, **60**, 447–458, doi: 10.1190/1.1443782.

Lakes R., 2009, Viscoelastic materials. Cambridge, ISBN 978-0-521-88568-3

Landau, L. D., and E. M. Lifshitz, 1986, Course of theoretical physics, Volume 7: Theory of elasticity, Third edition, Butterworth-Heinemann, ISBN 0 7506 2633 X

Matheney, M. P., and Nowack, R. L., 1995, Seismic attenuation values obtained from instantaneous frequency matching and spectral ratios: Geophysical Journal International, **123**, 1-15.

Mavko, G., 2013, Relaxation shift in rocks containing poroelastic pore fluids, Geophysics, **78**(3), M19-M28, doi: 1.1190 /GEO2012-0272.1

Morozov, I. B., 2008, Geometric attenuation, frequency dependence of Q, and the absorption band problem: Geophysical Journal International, **175**, 239–252.

Morozov, I. B., 2010a, On the causes of frequency-dependent apparent seismological Q: Pure and Applied Geophysics, **167**, 1131–1146, doi 10.1007/s00024-010-0100-6.

Morozov, I. B., 2010b, Attenuation coefficients of Rayleigh and Lg waves: Journal of

Seismology, 14, doi 10.1007/s10950-010-9196-5.

Morozov, I. B., 2011, Mechanisms of geometric attenuation: Annals of Geophysics, **54**, 235–248, doi: 10.4401/ag-4780.

Morozov, I. B., C. Zhang, J. N. Duenow, E. A. Morozova, and S. B. Smithson, 2008, Frequency dependence of regional coda Q: Part I. Numerical modeling and an example from Peaceful Nuclear Explosions. Bulletin of Seismological Society of America, **98**, 2615–2628, doi: 10.1785/0120080037.

O'Doherty, R. F., and Anstey, N. A., 1971, Reflections on amplitudes: Geophysical Prospecting, **19**, 430–458.

Sun, X., and L. N. Frazer, 2000**,** Shear wave attenuation profile from sonic dipole well-log data: Geophysical Research Letters, **27**, 285–288, doi: 10.1029/1999GL005423.

Suzuki, H., and J. Matsushima, 2013, Quantifying uncertainties in attenuation estimation at methane-hydrate-bearing zones using sonic waveform logs: Geophysics, **78**, D339–D353, doi: 10.1190/GEO2012-0495.1

Tisato, N., B. Quintal, S. Chapman, C. Madonna, S. Subramanyan, M. Frehner, E. H. Saenger, and G. Grassell, 2014, Seismic attenuation in partially saturated rocks: recent advances and future directions: The Leading Edge, **33**, 640-646.

Toksöz, M. N., A. M. Dainty, E. Reiter, and R. S. Wu, 1988, A model for attenuation and scattering in the earth's crust: Pure and Applied Geophysics, **128**, 81-100.

Virieux, J., and S. Operto, 2009, An overview of full-waveform inversion in exploration geophysics: Geophysics, **74**, WCC1-WCC26.

Wang, Y., 2008, Seismic inverse Q filtering, Blackwell, ISBN 978-1-4051-8540-0.

White, R. E., 1992, Accuracy of estimating Q from seismic data: Geophysics, **57**, 1508-1511.

Wu, R.-S., 1985, Multiple scattering and energy transfer of seismic waves, separation of scattering effect from intrinsic attenuation: Geophysical Journal Royal of Astronomical Society, 82, 57–80.

TABLES

Table 1. Characteristic time intervals required for spectral Q measurements

Measurement	Measurement time base (t), ms
VSP, $Q \approx 50$ with 30% error	27
VSP, $Q \approx 100$ with 30% error (White, 1992)	500
VSP, $Q \approx 160$ with 30% error	170
VSP, geometric attenuation $\gamma \approx 0.3$ s^{-1}, with 30% error	3600
Scattering Q	600-1200
Coda Q	700-1400
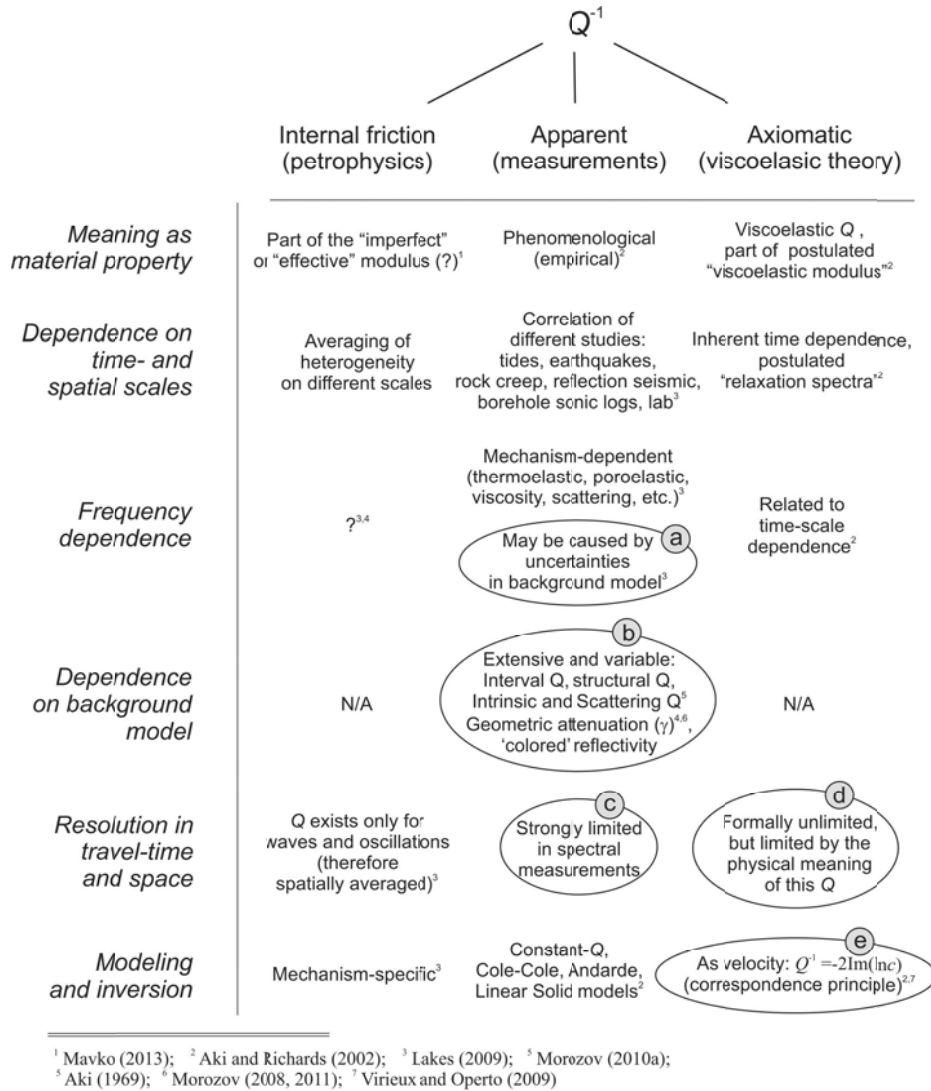
FIGURES

Figure 1. The discussed taxonomy of attenuation (Q^{-1}). Columns are the three general types of Q^{-1}, and rows (labeled on the left) are the aspects by which these types are differentiated. Ellipses labeled 'a-e' highlight the points discussed in the present paper, and footnotes refer to selected (incomplete) literature.

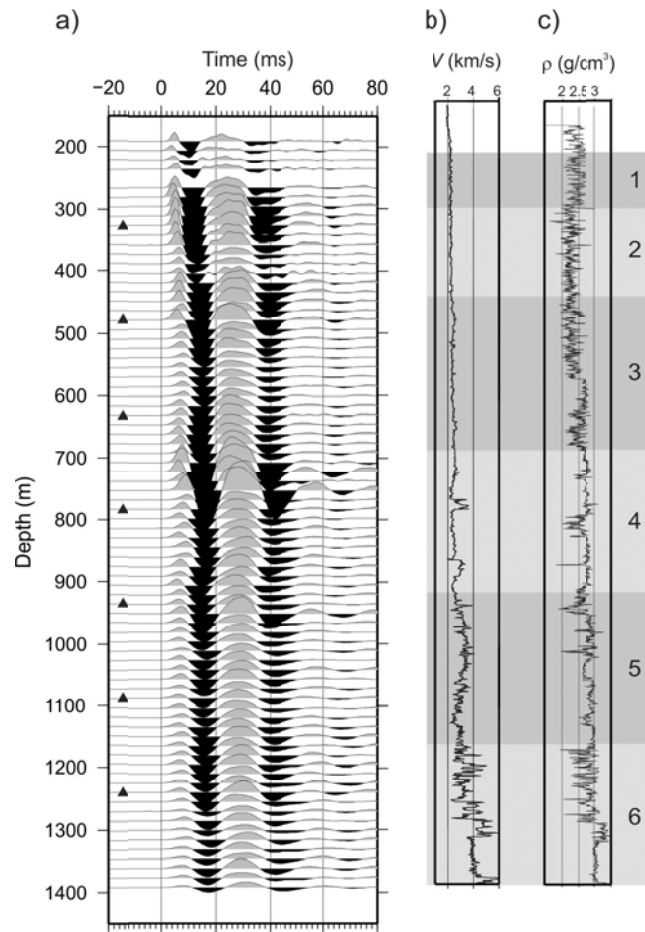Figure 2. Weyburn borehole data: a) Vertical-component records from a near-offset VSP shot aligned on the picked first arrivals, b) acoustic log and c) density log. In plot a), black triangles indicate the reference layers for coherency measurements (Figure 3). In b) and c), numbered gray-shaded depth intervals are the layers used in the attenuation inversion (BAM13).
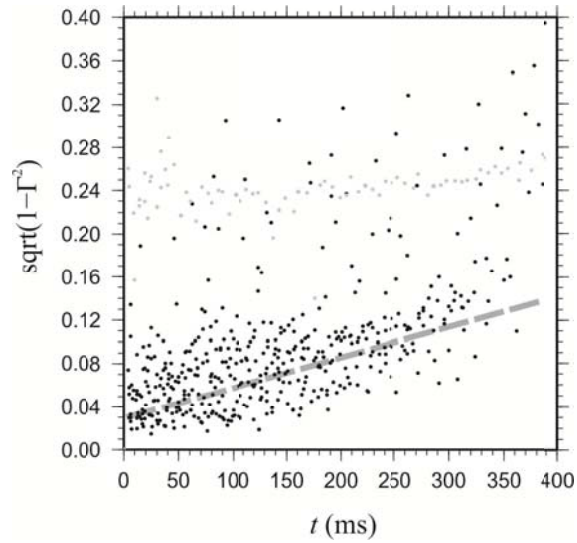
Figure 3. Spectral "incoherence" $\sqrt{1-\Gamma^2}$ coherence averaged within 80-Hz frequency band for first arrivals from the VSP shot in Figure 2. Seven reference levels were selected at the levels indicated by black triangles in Figure 2a. For the first arrivals recorded at each reference level, the values of $\sqrt{1-\Gamma^2}$ were measured with arrivals at all other depths and plotted against the first-arrival time differences, t. Black dots show the results for reference layers above 2200 m, and gray dots are the results for the reference level at 1239-m depth. Dashed gray line indicates an empirical linear trend used in resolution estimates.
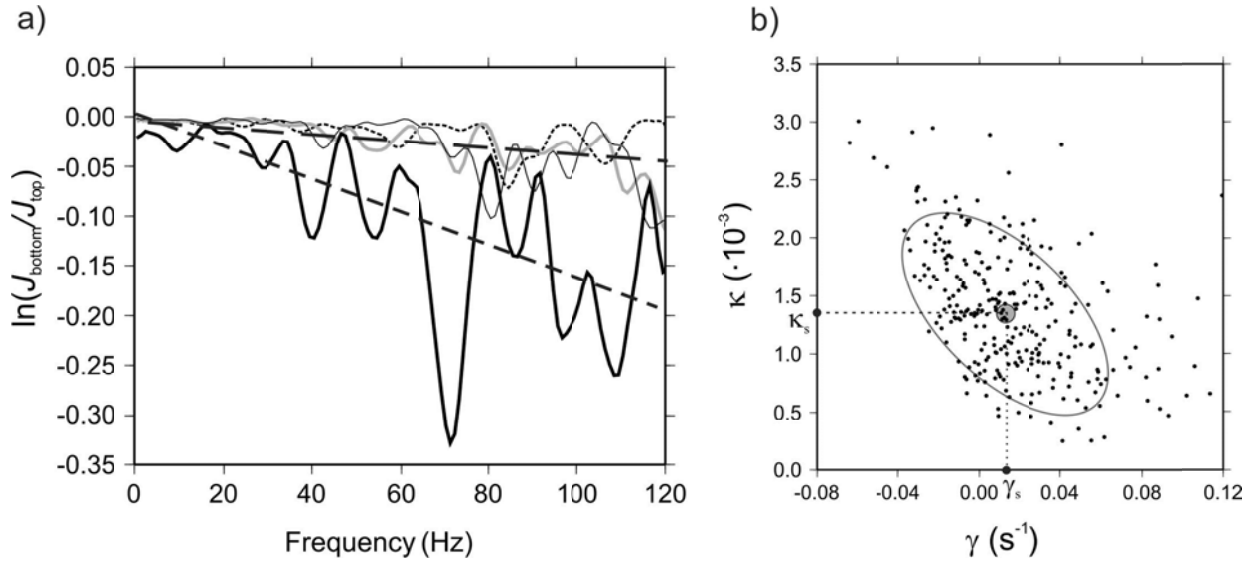
a)

b)

Figure 4. 'Structural' and 'scattering' Qs in the area of Weyburn VSP: a) Logarithms of the relative P-wave transmitted energy flux modelled by using the sonic log and density data within layer 3 in Figures 2b and c (thick black line) and three additional realizations of the same obtained by random permutation of the layers in the log (other lines). Long-dashed lines show linear dependences $\ln\left(J_{\text{bottom}}/J_{\text{top}}\right) \approx -\gamma - \kappa f$ for the non-randomized and a representative randomized case. b) Parameters $\hat{\gamma}$ and $\hat{\kappa}$ obtained for 300 random permutations of the logs in this depth interval. Small dots in plot b) can be viewed as the 'structural Qs', and the large dot (γ_s, κ_s) interpreted as the 'scattering Q'. The ellipse shows an estimate of the uncertainty in γ_s and κ_s with about 80% statistical confidence.
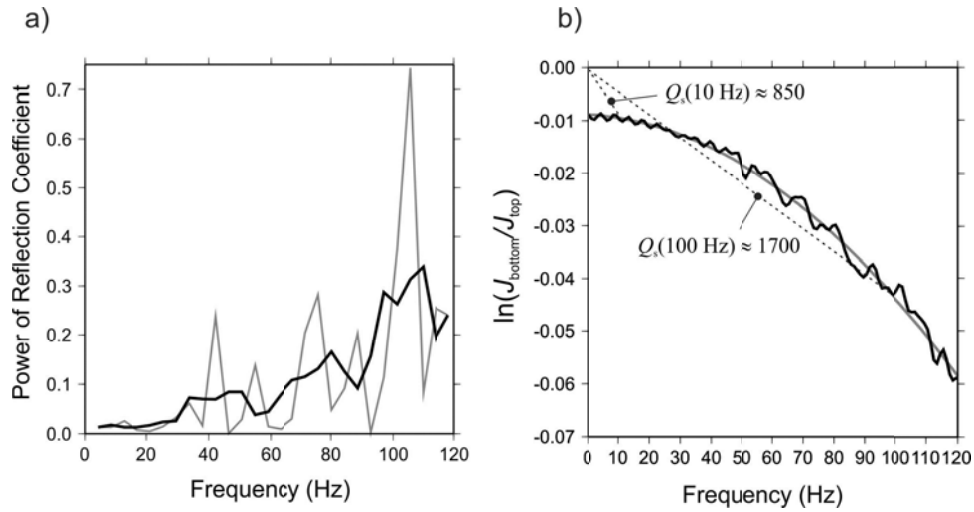
a)

b)

Figure 5. Modeled P-wave transmission through a 259-m segment of layering in the Weyburn VSP area: a) Raw (gray) and smoothed spectral power (black) of reflectivity within the same segment of the well log; b) Dependence of the logarithm of the downgoing energy flux on frequency after averaging 300 random permutations of the layers. The gray line shows a parabolic approximation for the amplitudes, and slopes of the dotted lines correspond to the apparent scattering Q_s at frequencies 10 Hz and 100 Hz.
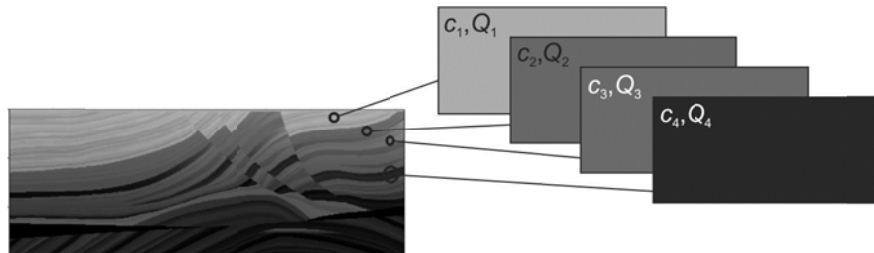

Figure 6. Seismic waveform modeling in a detailed Q model. For each point within the model (left), the Q (i.e., the stress-strain phase lag) is postulated to be the same as the apparent Q in an equivalent uniform medium (right) with complex phase velocity c^* equal the wave speed at the selected point (shades of gray). Note that these uniform-media Q's characterize harmonic plane waves and are therefore not localized in space.